Supporting Information

Porous Aluminum Electrodes with 3D Channels and Zig-Zag Edges for Efficient Hydrogen Evolution

Arun Prakash Periasamy,‡[a] Pavithra Sriram,[b] Yu-Wen Chen,[a] Chien-Wei Wu,[a] Ta-Jen Yen,[b] and Huan-Tsung Chang*[ac]

[a]Department of Chemistry, National Taiwan University, 1, Section 4, Roosevelt Road, Taipei 106, Taiwan.

[b]Department of Materials Science and Engineering, National Tsing Hua University, Hsinchu 30013, Taiwan.

[c]Department of Chemistry, Chung Yuan Christian University, Chung Li District, Taoyuan City, 32023, Taiwan.

‡ Present address: School of Engineering and Materials Science, Queen Mary University of London, Mile End Road, London E1 4NS, England, UK.

Corresponding Author: Professor Huan-Tsung Chang, Department of Chemistry, National Taiwan University, 1, Section 4, Roosevelt Road, Taipei 10617, Taiwan. Tel and fax: 011-886-2-33661171. E-mail: changht@ntu.edu.tw

Experimental

Materials

Aluminum foil (7.62 m x 30.4 cm) with 0.1 mm thickness was purchased from Reynolds Consumer Products (Richmond, VA, USA). Sodium hydroxide pellets were purchased from Macron Fine Chemicals (PA, USA). Sulfuric acid (97%) was purchased from Echo (Miaoli, Taiwan). Nitric acid (69%) was obtained from Applichem Panreac (Barecelona, Spain). Cesium chloride (CsCl; 99%) and sodium bromide (NaBr; 99.5%) were procured from Acros Organics (Geel, Belgium). Sodium chloride (NaCl; >98%), calcium chloride dihydrate ($CaCl_2 \cdot 2H_2O$) (98%) and sodium iodate ($NaIO_3$; 99%) were purchased from Sigma Aldrich (St. Louis, MO, USA). Sodium fluoride (NaF; 97%) was obtained from Wako Pure Chemicals (Osaka, Japan). Sodium nitrate ($NaNO_3$; 99.5%) was purchased from J. T. Baker (Center Valley, PA, USA). Sodium aluminate ($NaAlO_2$; Al_2O_3: 51-55%, Na_2O: 38-42%), and sodium iodide (NaI; 99%) were purchased from Showa (Tokyo, Japan). Lithium chloride (LiCl; 99%) and barium chloride ($BaCl_2 \cdot 2H_2O$; 99%) were purchased from Merck (Kenilworth, NJ, USA). Rubidium chloride (RbCl; 99%) was procured from Riedel-de Haën (Sleeze, Germany). All solutions were prepared using ultrapure water obtained from a Milli-Q ultrapure (18.2 MΩ cm) system.

Characterization

The morphology of as-prepared aluminum electrodes was recorded using a Hitachi S-2400 scanning electron microscope (Hitachi High-Technologies, Tokyo, Japan) equipped with an energy-dispersive X-ray spectrometer (EDS). X-ray diffraction (XRD) patterns of all aluminum electrodes were recorded using a PANalytical X'Pert PRO diffractometer from PANalytical B.V. (EA Almelo, Netherlands) and Cu-Ka radiation (λ = 0.15418 nm). CHI 760D electrochemical work station was used to record the electrochemical impedance spectra (EIS) and the Nyquist plots

of the aluminum electrodes in the frequency range 0.1 Hz to 10000 Hz at an amplitude of 5 mV in N_2 saturated 1 M H_2SO_4.

Preparation of porous aluminum electrodes

Porous aluminum electrodes were prepared through an electrochemical anodization process. Prior to electrochemical anodization, the aluminum foils (4 x 2.5 cm) were soaked in NaOH solution (100 mL, 0.1 M) for 5 min and then washed with ultrapure water. The treated aluminum foils were soaked in HNO_3 solution (100 mL, 0.5 M) for 5 min and then etched in the vertical direction to form channels. After each pretreatment step, the foils were rinsed with ultrapure water and the excess water was wiped off with tissue paper. The pretreated aluminum foils were then subjected to electrochemical anodization in solutions containing NaCl (20 mL, 60 mM) at 6 V respect to an Ag/AgCl reference electrode for 80 s to form porous structures. A platinum wire was used as a counter electrode. The reference electrode and working electrode were kept as close as possible to minimize the ohmic drop. The area (2.5 x 1.5 cm) of the aluminum foil (electrode) exposed to the electrolyte was kept constant and it was considered as the final working area. Instead of NaCl solution, solutions containing different salts were used to prepare porous aluminum foils. After each anodization step, the foils were removed from the electrolytes and washed with ultrapure water. The excess water on the electrode surface was wiped off with tissue paper.

Electrocatalytic and photocatalytic hydrogen evolution

The activities of bare aluminum electrode, the pretreated aluminum electrode, and the porous aluminum electrodes for HER were measured in N_2 saturated H_2SO_4 solution (20 mL, 1M). Prior to use, the electrolyte solution was purged with N_2 for 45 min. All voltammograms were recorded in H_2SO_4 solution with N_2 purging to maintain inert atmosphere and efficient mass

transport. For each electrode, 20 cyclic voltammetry (CV) scans were recorded over the potential range from 0.08 to -0.82 V vs. reversible hydrogen electrode (RHE) at a scan rate of 100 mV s^{-1}. Linear sweep voltammograms (LSVs) were then recorded over the potential range from 0.08 to -0.82 V at a scan rate of 5 mV s^{-1}. The potential of the porous aluminum electrode at the benchmarking current density of 10 mA cm^{-2} was measured.

Photoelectrochemical response of the porous aluminum electrode at a fixed overpotential of 0.82 V was measured under chopped illumination. A 500 W UV–vis lamp (Newport, Oriel Instrumentation, Irvine, California, USA) as a light source emitting light in the wavelength range of 400–1100 nm was used. The distance between the light source and the porous aluminum electrode was 10 cm.

ESI note 1:

Formation and characterization of porous aluminum electrode

The bare aluminum foil is treated with NaOH and then the as-formed oxide layer on the surface is removed using HNO_3 to generate a honeycomb like porous surface with vertical channels. In the NaOH solution, the hydroxide ions diffuse and adsorb onto the aluminum surface, leading to the formation of sodium aluminate and hydrogen as shown in equation (1). [1]

$$2Al + 2NaOH + 6H_2O \rightarrow 2Na[Al(OH)_4] + 3H_2 \uparrow \Delta H^o_{298} = -831.2\ kJ\ mol^{-1} \quad (1)$$

In the HNO_3 solution, vertical and horizontal etching of aluminum atoms is enhanced, resulting in the formation of vertical channels and honeycomb like pores. When applying an anodic

potential (6V), the aluminum electrode oxidizes to form Al^{3+} ions. Some of the released Al^{3+} ions in the bulk solution react with water molecules to form $Al(OH)_3$. At the cathode, the reduction of protons leads to the formation of hydrogen. In the solution containing NaCl (pH 8.0), the positively charged aluminum surface (isoelectric point ~9.0) attracts Cl^- ions.[2] During the reaction course (80 s), more Cl^- ions diffuse through the vertical channels and honeycomb like pores, leading to increased localized dissolution of aluminum atoms by corrosion or crystallographic pitting corrosion to form defects, pores and channels.[3, 4] We note that the pores are formed through crystallographic/or cubic pitting along (100) facets, while the channels are formed through vertical etching along (111) facets.

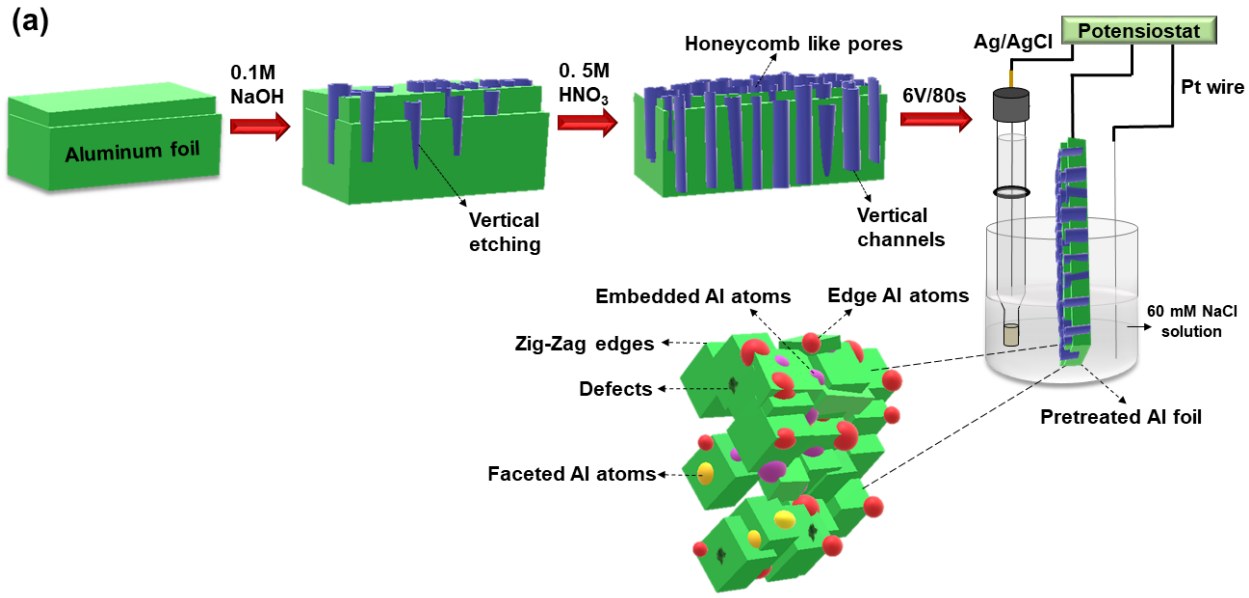

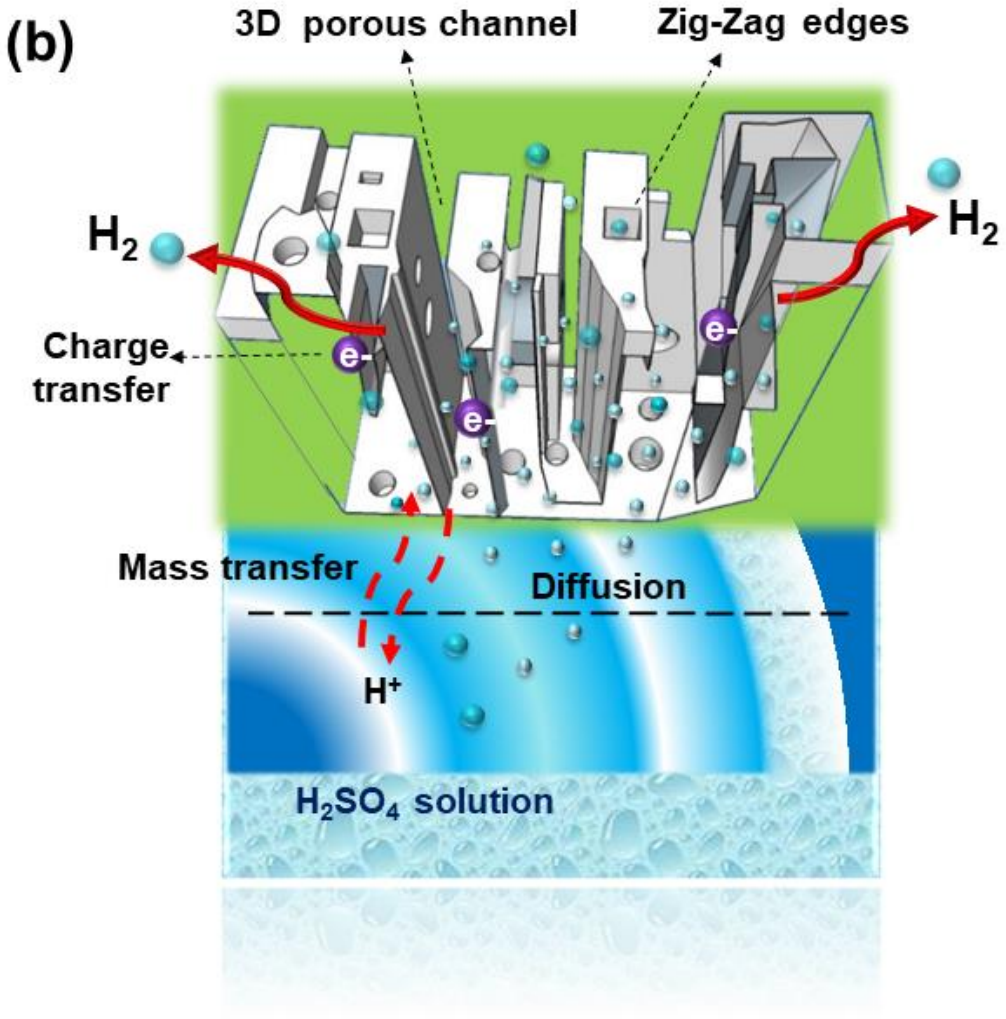

Scheme S1. Synthesis of a porous aluminum electrode for the generation of hydrogen from aqueous solution. (a) Processes for the formation of porous aluminum electrode with defect, zig-zag edges, and channels. (b) The porous structure facilitates charge transfer, mass transport, and diffusion, leading to greater HER efficiency.

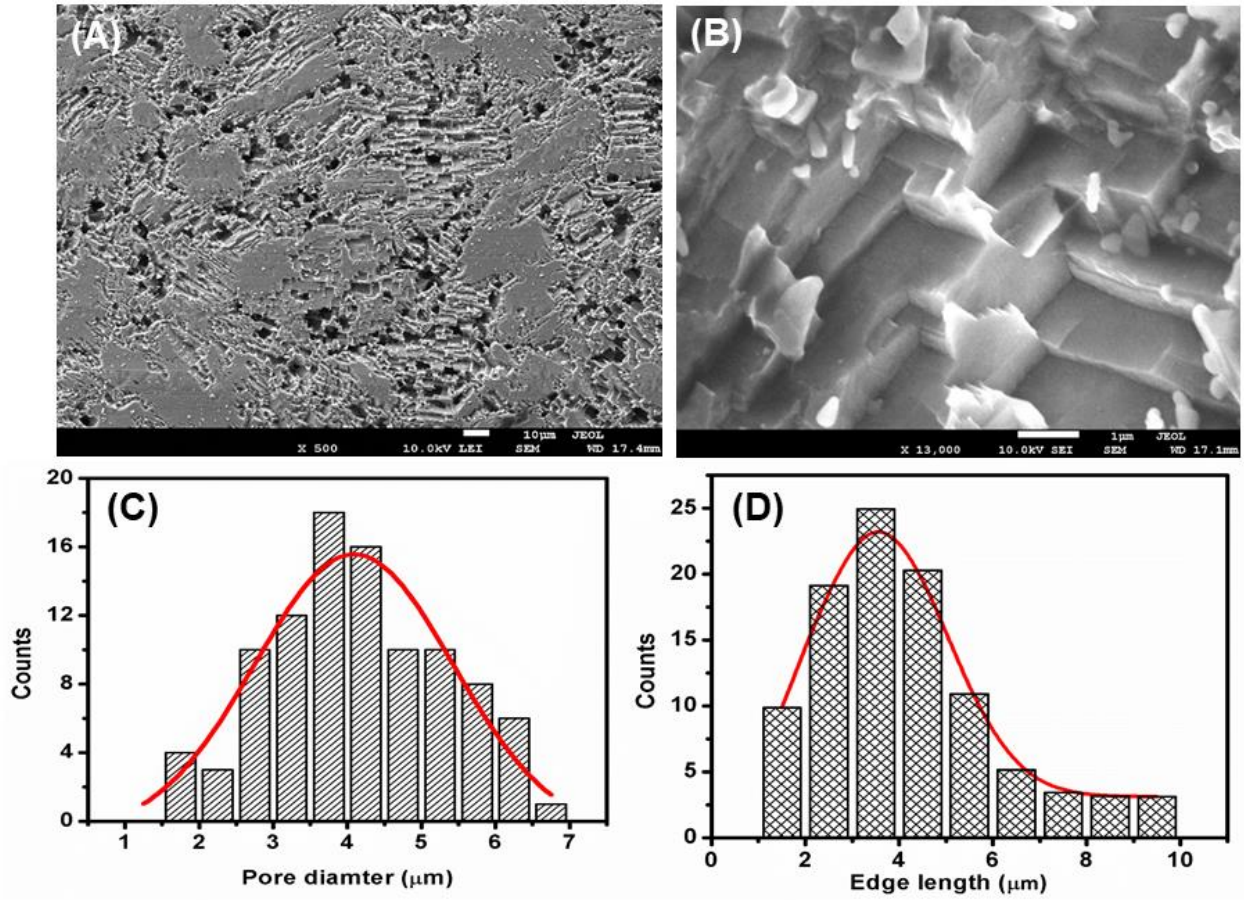

Fig. S1 SEM image (A), magnified SEM image (10-fold) showing zig-zag active edges (B), pore size histogram (C), and edge length histogram (D) of a representative BAA aluminum electrode prepared in 60 mM NaCl at 6 V for 80 s.

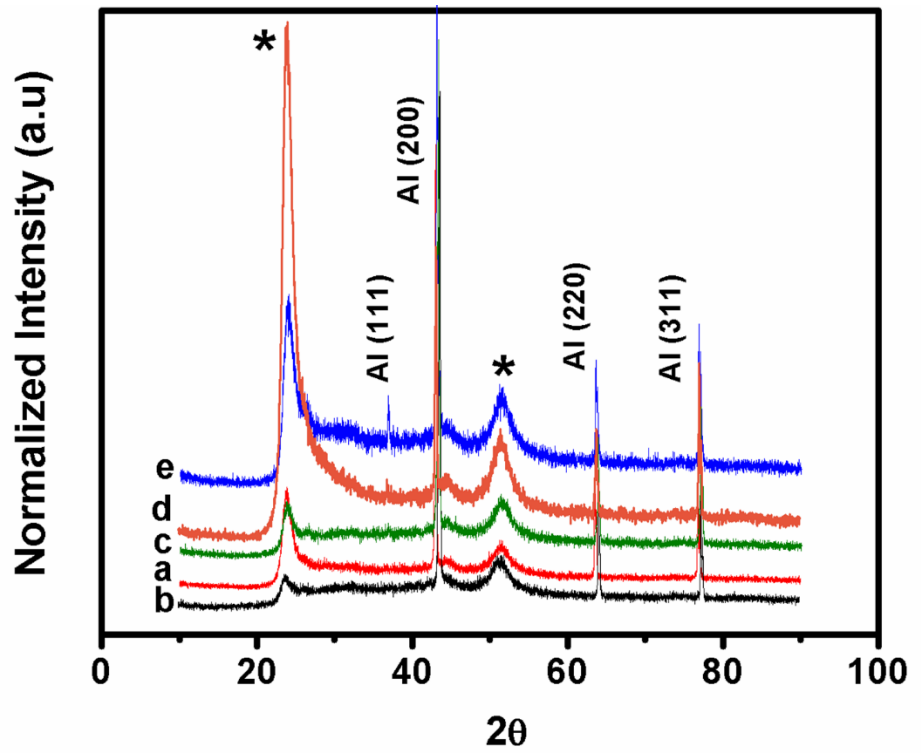

Fig. S2 XRD patterns of aluminum foils (a) without and with being treated with (b) 0.1 M NaOH, (c) 0.1 M NaOH/0.5 M HNO_3, (d) 0.1 M NaOH/0.5 M HNO_3/anodization, and (e) that prepared in (d) after ADT. ADT was conducted over the potential range from 0.08 to -0.82 V at a scan rate of 100 mV s^{-1} in N_2 saturated 1 M H_2SO_4. Other conditions are the same as shown in Fig. 1. The signals denoted as asterisks (*) are from the stainless steel sample holder.

ESI note 2:

Parameters controlling the morphology and electrochemical activity of porous aluminum electrode

At a constant potential (6V) of anodization for 80 s, the effects of NaCl (1 to 100 mM) on the preparation of BAA aluminum electrodes and their activities were tested. Upon increasing the NaCl concentration (1-60 mM), the activity of the electrodes enhanced as shown in **Fig. S3A**, mainly due to increased numbers and sizes of pores, 3D channels, and zig-zag edges,[2] with a support of the SEM images displayed in **Fig. S4**. To reach the current density of 10 mA cm^{-2}, the BAA aluminum electrodes prepared in 10, 30, 60, 80, and 100 mM NaCl provided the overpotentials of 0.82, 0.77, 0.58, 0.77, 0.75 V, respectively. Their pore diameters are 0.33, 2.78, 3.2, 7.31, and 15.98 μm, respectively. The electrochemical activity of the BAA electrodes prepared at NaCl concentrations higher than 60 mM decreases upon increasing NaCl concentration, mainly because of less aluminum on the electrode. Based on the electrochemical activity of the BAA aluminum electrodes, the optimal NaCl concentration was found to be 60 mM.

Fig. S3B displays that the applied potential for anodization is important in determining the electrochemical activity of porous aluminum electrodes. In solutions containing NaCl (60 mM), the applied voltage of 6 V is more suitable than 3 and 10 V when the anodization was conducted for 80 s. Upon increasing the applied voltage, the reaction rate increases, leading to increased dissolution of aluminum and thus greater numbers and sizes of pores, 3D channels, and zig-zag edges (not shown). At 10 V, less aluminum left on the electrode is responsible for the loss in its electrochemical activity. At a constant voltage (6V) and constant NaCl concentration (60 mM), we then tested the effect of anodization time as shown in **Fig. S3C**. Upon increasing the reaction time, larger sizes and numbers of pores, 3D channels, zig-zag edges were formed (not shown),

leading to increased electrochemical activity of the BAA aluminum electrode. However, less aluminum on the electrode is again responsible for the loss of its activity when anodization time is longer than 80 s.

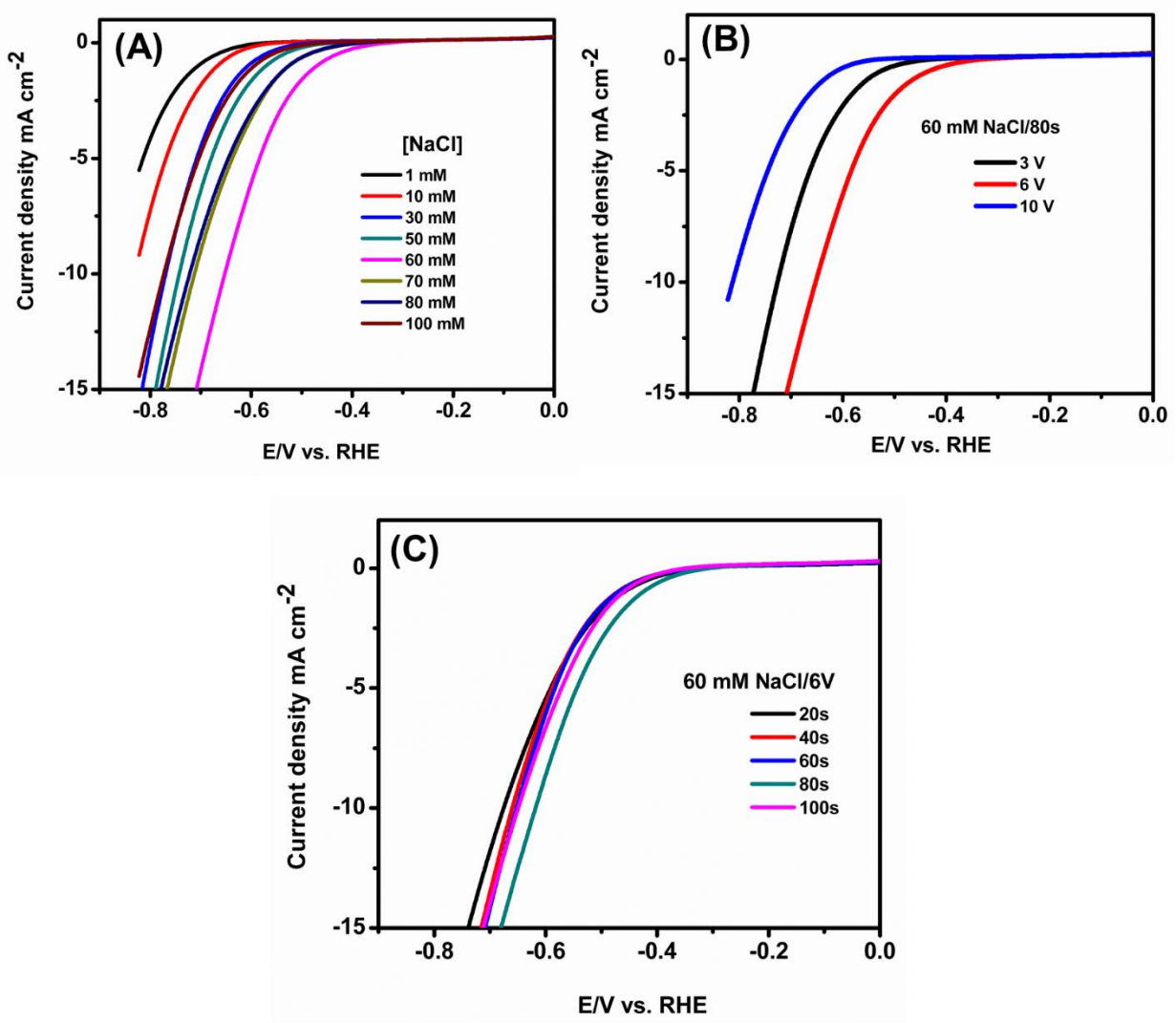

Fig. S3 Optimal conditions for preparation of BAA aluminum electrodes. Effects of NaCl (A), applied potential (B), and anodization time (C).

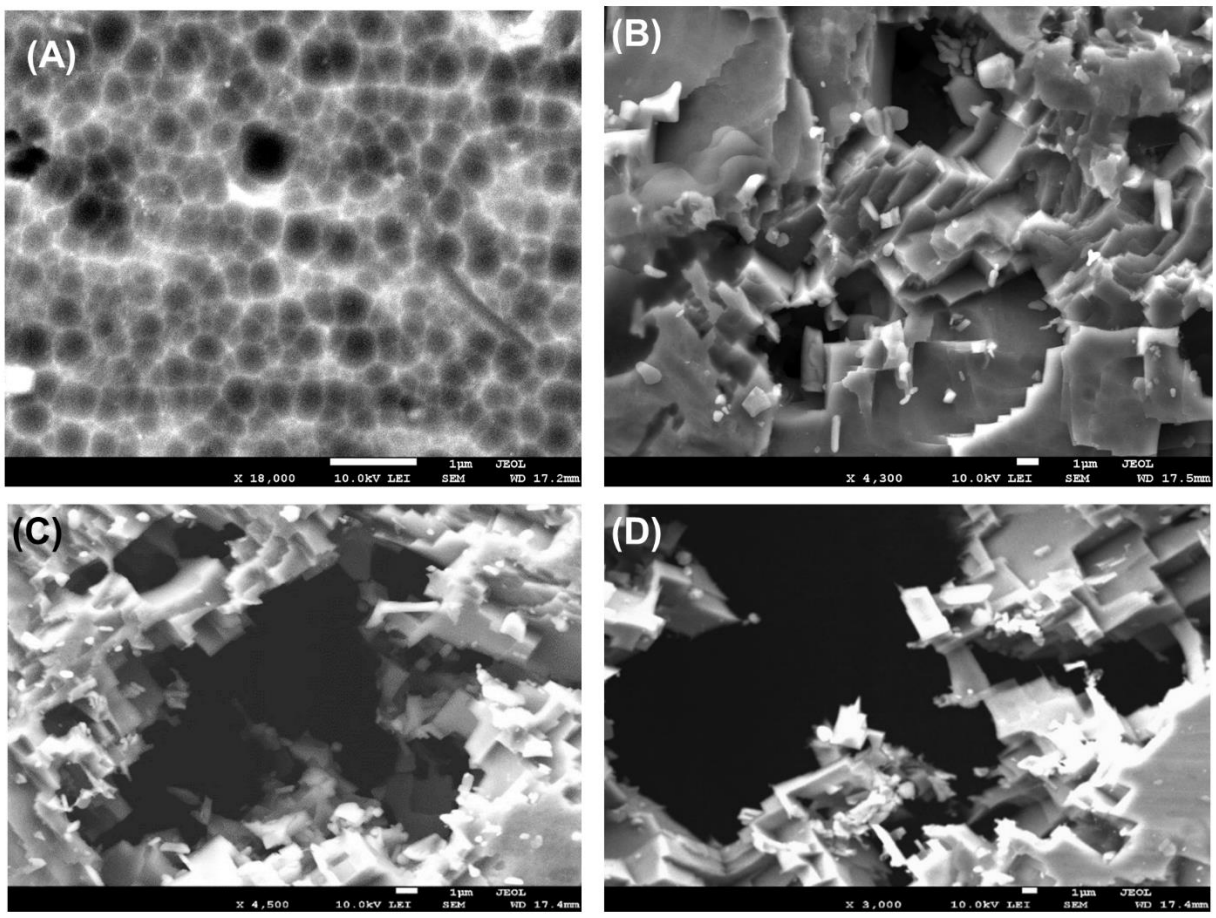

Fig. S4 SEM images of the BAA aluminum electrodes prepared in aqueous solutions containing various concentrations of NaCl at 6 V for 80 s. NaCl concentrations (mM): 1 (A), 30 (B), 80 (C), and 100 (D).

ESI note 3:

Effect of cations and anions on the anodization and the activity of BAA electrodes

The electrode prepared in sodium fluoride solution exhibits the lowest activity due to the greater covalent character and the stronger adsorption of F^- anions on the electrode surface.[5] Compared to Br^- and I^-, Cl^- is smaller in size and thus has greater migration efficiency, lower specific adsorption capacity, and lower interaction energy with the solvent molecules. Chlorides efficiently diffused through the defects and reacted with the Al^{3+} cations in lattice or that in pits to form pores, 3D channels and zig-zag edges, leading to higher catalytic activity. SEM images and mappings of elements of BAA aluminum electrodes prepared in NaF, NaCl, NaBr, NaI, and, NaClO are displayed in **Fig. S5** to support our reasoning. The EDX spectra **(Fig. S6)** of the BAA aluminum electrodes prepared in sodium salts revealed the presence of various amounts of Al (90-98%). Because of the higher crystallographic pitting efficiency of Cl^- anions, greater formation of exposed active sites (edges) was observed **(Fig. S6B)**. The electrode prepared in NaClO (a strong oxidizing agent) provided lower activity than that prepared in NaCl, but higher than the other sodium halides, suggesting that the oxidizing agent had no significant role playing in the formation of pores and 3D channels. It is of note that the electrode prepared in $AlCl_3$ than that in $NaAlO_2$ provided higher electrochemical activity, supporting the important role of Cl^- playing in etching the aluminum electrode and thus its activity.

The HER onset potentials of the electrodes prepared in various metal chloride salts decreases in the order of NaCl < CsCl < LiCl < RuCl < KCl < $CaCl_2$ < $BaCl_2$ < $MgCl_2$. Compared to the alkaline metal cations, the alkali metal cations possess smaller atomic radii and thus they diffuse quickly through the electrolyte and adsorb on the cathode surface or within the electrical

double layer.[6] On the other hand, an anion toward the anode is faster if its interaction with solvated cations is weaker, leading to faster anodization speed. In other words, more pores, 3D channels, and zig-zag edges were formed in the BAA aluminum electrode. The HER onset potentials of the electrodes anodized with the sodium anions decrease in the order of NaCl << $NaBrO_3$ < $NaIO_3$ < Na_2SO_4 < $NaNO_2$ < $NaNO_3$ < Na_2SO_3. Again, the result supports that anions play an important role in determining the structure and thus the activity of as-formed porous BAA electrodes. We also point out that the differences in the specific adsorption capacity of the test anions is also responsible for various hydrogen overpotentials.[7] Once the anions adsorbed on the electrode surface, the nature of potential distribution in the metal-electrolyte boundary changed. Among the tested anions, Cl^- has the highest affinity toward Al, and thus greater local Cl^- concentration is generated on the boundary, leading to lower hydrogen overpotential.

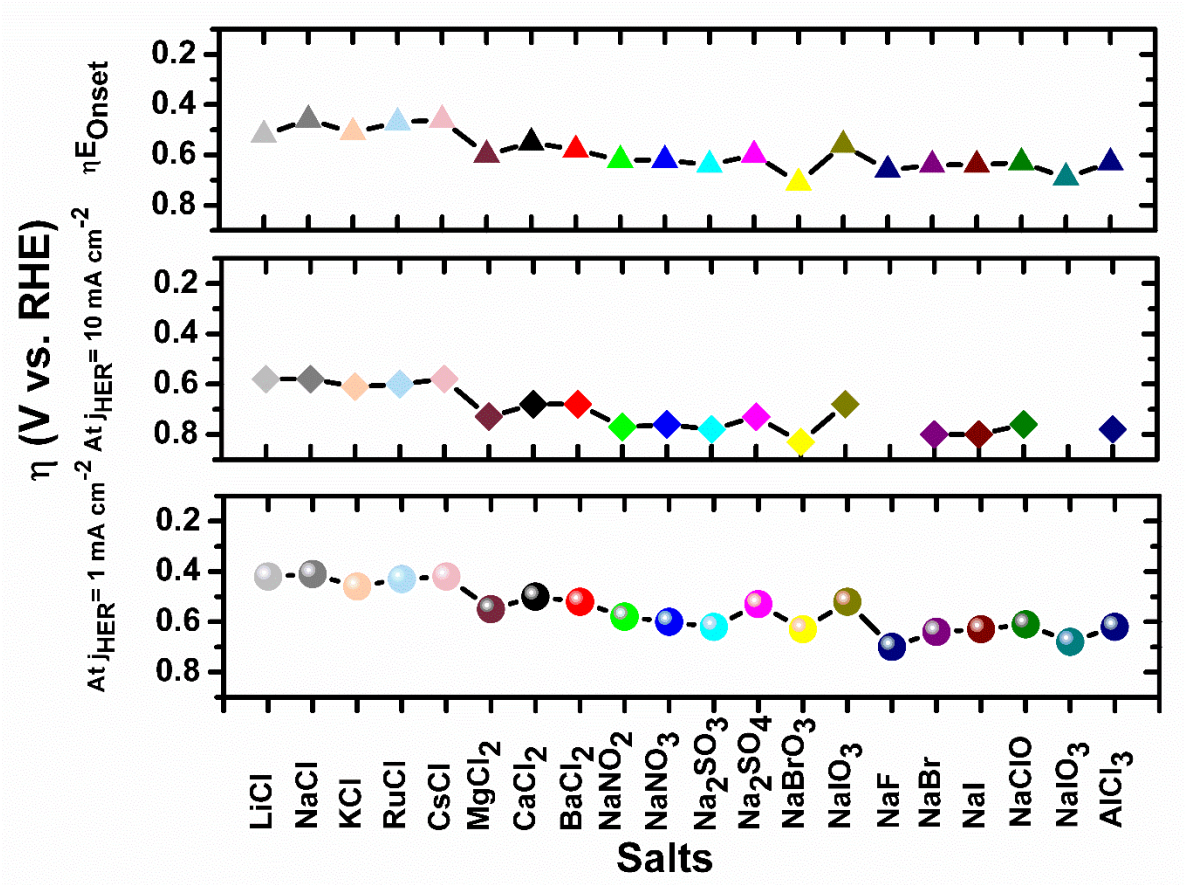

Fig. S5 Effect of alkali, alkaline metal cations and anions on the anodization of aluminum electrodes and their catalytic activity toward HER. The data were obtained from LSV curves that were recorded at a scan rate of 5 mV s^{-1} in N_2 saturated 1M H_2SO_4.

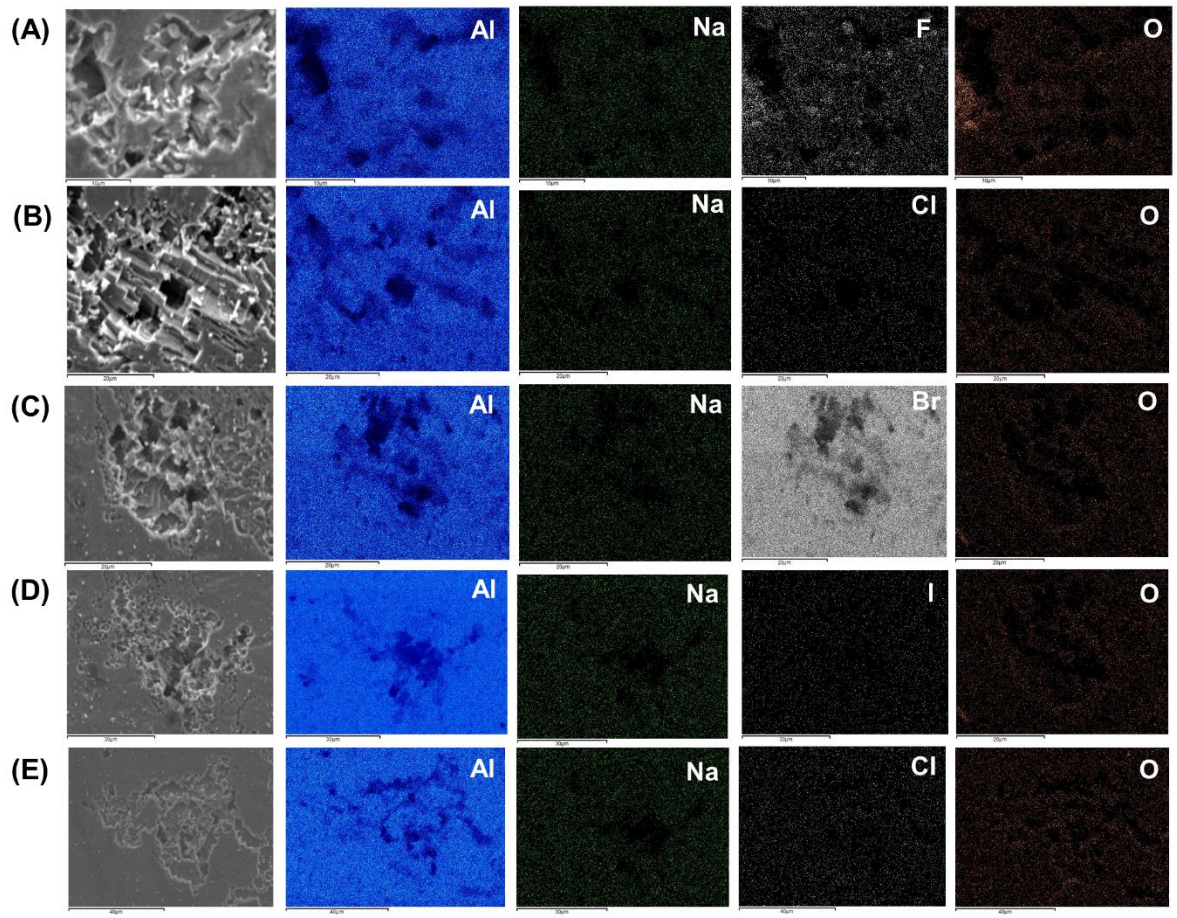

Fig. S6 SEM images and elemental mappings of the BAA aluminum electrodes prepared in various sodium halides (60 mM) at 6V for 80s. NaF (A), NaCl (B), NaBr (C), NaI (D) and, NaClO (E).

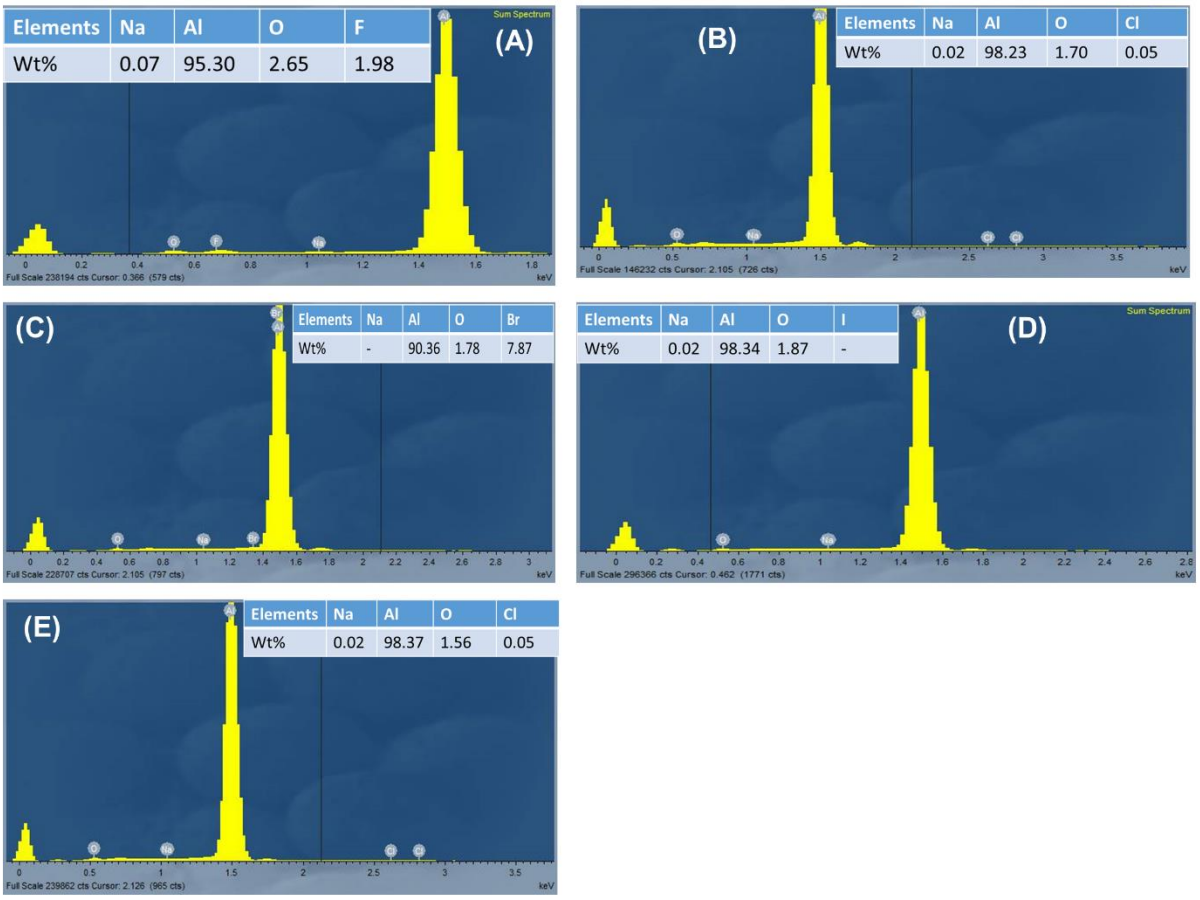

Fig. S7 EDX spectra of the BAA aluminum electrodes prepared in various sodium halides (60 mM) at 6 V for 80 s. NaF (A), NaCl (B), NaBr (C), NaI (D) and, NaClO (E). Insets to (A-E): elemental compositions in weight%.

ESI note 4:

Effect of pH on the activity of porous aluminum electrodes

We first tested the effect of pH on the activity of porous aluminum electrodes for HER. The onset potentials obtained in 1.0 M H_2SO_4 adjusted with various volumes of 15 M NaOH to pH 2.0, 4.0, 6.0, and 8.0 are -0.41, -0.64, -0.87 and -0.77 V respectively. In the low pH range (2.0-4.0), the onset potentials (negative values) are lower due to the improved proton transport through the pores and 3D channels. In the high pH range (4.0-11.0), $Al(OH)_3$ were formed on the surface, leading to higher onset potential for HER.[15] Relative to Al, $Al(OH)_3$ is less active, mainly because of its high passivity, resistivity, and low solubility.

Stability of the porous aluminum electrodes

The stability of the BAA aluminum electrode was tested at a fixed overpotential of 0.47 V in 1 M H_2SO_4 solution for 1 h. There was a slight drop in the current density within the first 500 s and thereafter it remained stable at a current density of 6.9 mA cm^{-2} as shown in **Fig. 3A.** The current densities at 2000, 3000 and 3600 s are 6.9, 6.6 and 6.3 mA cm^{-2}, respectively. The activity remained at least 91% after 1 h, showing good stability of the electrode for HER (**Fig. 3B)**. LSV curves were recorded after different cycles of ADT in 1 M H_2SO_4 as shown in **Fig. 3C**. The onset potential shifted to positive values within the first 400 cycles and thereafter it remained stable up to 900 cycles. Similar trend was observed when LSV curves were recorded after different cycles of ADT in 0.5 M H_2SO_4 as shown in **Fig. 3D**. The positive shift in the onset potential values regardless of the ionic strength might be due to the formation of thin oxide layer at the electrolyte/electrolyte interface that was then removed with further cycling in acidic solution.[8, 9] In other words, self-activation of the active sites in acidic medium leads to improved catalytic activity

and stability. SEM images of the BAA aluminum electrodes after 20, 400, and 900 cycles of ADT in 0.5 and 1 M H_2SO_4 solutions are displayed in **Fig. S8** to support our reasoning. It can be seen that most of the zig-zag edges were retained after 900 cycles of ADT, regardless of the ionic strength. Honeycomb like pores were created on the zig-zag edges, which likely enhanced the diffusion and mass transport and shifted the onset potentials to positive values. Thus, it is suggested to conduct ADT treatment prior to use for HER.

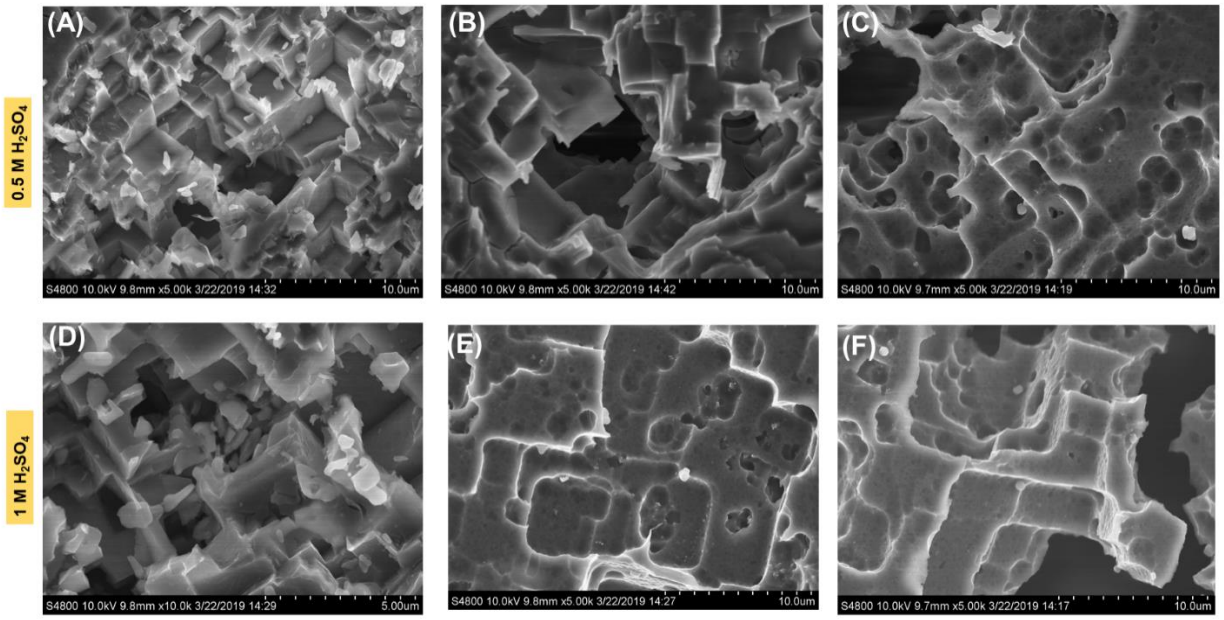

Fig. S8 SEM images of the BAA aluminum electrodes after 20 cycles (A, D), 400 cycles (B, E), and 900 cycles (C, F) of ADT in 0.5 M H_2SO_4 and 1 M H_2SO_4, respectively.

Comparison of stability and hydrogen production yield of the porous aluminum electrode with alloys and composites of Pt and aluminum

Table S1 provides a comparison of cycling stability and the hydrogen yield of the porous electrode to that of reported Pt-based nanocomposites, porous aluminum and aluminum-based alloys (ESI-Note 4). It is of note that the most reported Pt and Pt-based composites maintained good cycling stability in acidic media with low (0.1-0.5 M) and high ionic strength (1 M).[10-13] Over the cycle range (100 to 2000), tested electrodes retained initial currents with negligible shifts in their onset potentials. For the BAA aluminum electrodes, the onset potentials shifted to positive values after 900 cycles regardless of the ionic strength, mainly due to the self-activation of their active sites and their honeycomb like pores formation, as revealed from SEM images displayed in **Fig. S8**. Additionally, surface oxides formed on the catalyst surface were peeled off by hydrogen bubbles while cycling in acidic medium, which offered extra actives sites to display higher catalytic activity compared to their initial states.[14] Most importantly, a significant decrease in overpotential to reach 10 mA cm^{-2} with an increase of CV cycling was noted. In other words, self-activation of the aluminum surface and zig-zag sites minimized the energy needed for hydrogen production. On the other hand, the PtCuNi/Carbon nanofiber array @carbon felt monoliths exhibited small negative potential shifts after 2000 cycles.[15] It is of important note that there was an 18% current loss after conducting chronoamperometry test at this electrode for 1000 s, while commercial Pt/C electrode lost its 37% initial current. Interestingly, BAA electrode exhibited only 9% current loss after conducting chronoamperometry test at a relatively higher overpotential (470 mV) for 3600 s, showing its good stability. It has to be noted that Pt composites listed in Table S1 were prepared by using several sophisticated instruments, and by applying high temperature, high voltage, high pressure and time consuming multiple step processes (2-24 h). Moreover, the production costs of

Pt nanoparticles (4-150 nm) and Pt-based alloys/composites is high, 10-100 USD per m^{-2}, while the preparation costs of 10 nm to 1 µm thick Pt thin films are much higher, 100-1000 USD per m^{-2}.[10] With the advantages of low cost (2-3 USD per 25 m long rolls) and abundance, aluminum electrodes (20-50 cm long), commercial aluminum powders and different aluminum alloys (0.5-1.0 g) were used to generate hydrogen in neutral (water) or basic media.[16-19] Although hydrogen yields were high (40-75 mL min^{-1} g^{-1}), corrosion, passivation and rapid loss of chemical activity due to the formation of surface oxides and hydroxides are problematic. Their preparation requires critical conditions such as inert atmosphere and high temperature (800-900 ^{o}C), and/or complicated processes.[20] Moreover, aluminum alloys must be stored under liquid nitrogen to remain the chemical activity.[17] On the other hand, BAA electrodes were prepared within a short time (80 s) from low cost aluminum foils (2-3 USD per 25 m long rolls) using a simple potentiostat, non-toxic salt (NaCl) and less voltage (6 V) without requirement of any inert storage conditions. The hydrogen production using the BAA electrodes is thus simple, fast and cost-effective. It produced 7.5 mL hydrogen in 1 h at an overpotential of 1.35 V vs. RHE in a custom built electrochemical cell containing a litre of 1 M H_2SO_4, as shown in **Fig. S9**. The electrode size used in this study is relatively much smaller than that used in previous reports (2.5 cm long vs 20-49.5 long), and thus comparison of our hydrogen yield with that reported is difficult. The porous aluminum electrode is relatively stable; negligible damage of the electrode surface was found after 1-h electrolysis in a custom built electrochemical cell with a higher electrolyte capacity (1000 mL 1 M H_2SO_4), showing its potential use in large scale hydrogen production (**Fig. S9B**). The hydrogen yield and formation rate can be increased by increasing the working areas of the porous aluminum electrode and the anode, number of active zig-zag edges, channels, pores and the catalytic active sites per unit area of the porous aluminum electrode. We believe that the electrochemical deposition of

highly active inexpensive transition metals and their alloys on active edges of porous aluminum electrode would further stabilize the active edges and boost the hydrogen production yield and stability.

Table S1 Comparison of stability and hydrogen production yields of porous aluminum electrodes with that of reported alloys and composites of Pt and aluminum.

Electrodes/ Materials	Synthesis method (condition)	Shape, size, (loading)	Electrolyte H_2SO_4 (M)	Stability (CV cycles)	Hydrogen yield (mL/h)	Ref.
Pt/tungsten monocarbide	physical vapor deposition assisted magnetron sputtering (1000 ^oC under hydrogen and methane atmosphere) coupled thermal evaporation	monolayer, thin film	0.5	stable (25)	[a]NA	[10]
Pt/polyacrylonitrile	hydrothermal (80 ^oC, 6 h), electrospinning (voltage**:**12 kV, flow rate: 60 µL/h; distance: 12 cm), stabilization (280 ^oC, 6 h), and carbonization (1000 ^oC, 8h)	nanoparticles, 2.2 nm, (6 wt% loading) nanofibers	0.5	stable (1000) chronoamperometry : stable (-0.25 V vs. RHE for 12 h)	NA	[11]
PtCuNi/Carbon nanofiber array @Carbon felt monolith	hydrothermal (120 ^oC/ 12 h), thermal activation (420 °C for 12 h), catalytic decomposition of methane (600 °C for 4 h), and galvanic displacement reaction (40 °C for 2 and 24 h)	nanoparticles on fibers (Cu: 56.8; Pt: 42.1% and Ni: 1.1%)	1.0	small negative potential shifts (2000) chronoamperometry : current loss (18% vs. 37%, for commercial Pt/C) after 1000 s	NA	[15]
Atomic layer deposited Pt/nitrogen-doped graphene nanosheets	graphite exfoliation (1050 ^oC under Ar), post-heating (900 ^oC for 10 min under Ar/NH_3), and atomic layer deposition (250 ^oC for 1 to 5 s)	single atoms, clusters	0.5	4% current loss at 0.04 V vs. RHE (1000)	NA	[12]
Pt-TiO_2-nitrogen doped reduced graphene oxide	graphene oxide synthesis (80 ^oC for 30 min), hydrothermal synthesis of nanocomposites (225 ^oC for 24 h), and photodeposition of Pt nanoparticles (UV irradiation for 5 h)	cuboid faceted anatase TiO_2 NCs, 100-150 nm; Pt nanoparticles, 2-10 nm (~3 µg)	0.1	stable (100); overpotential increased by 1.2 mV at a current density of 86 mA cm^{-2}	NA	[13]

$NiS_2@Al_2O_3$ nanosheets	hydrothermal (180 ^oC, 18h), post treatment (750 ^oC, 3.2 h), and calcination at 400 ^oC, 3.2 h)	nanosheets, microflower, ~2 µm	0.5	stable (2000); chronoamperometry : current loss (3% @10 and 20 mA cm^{-2}; stable for 48 h)	NA	[21]
Al	commercial/waste water electrohydrolysis using photovoltaic cells	rod ([b]L = 49.5 cm; [c]D = 0.9 cm)	waste water	NA	680	[22]
Al electrodes	commercial/waste water electrohydrolysis coupled chemical oxygen demand removal	rod ([b]L = 20 cm, [c]D = 0.4 cm)	olive mill wastewater	NA	0.125 @ 0.5 V 25 @ 2V 32 @ 3V	[23]
Al powder	ball milling (Al powder and NaCl) at 270 rpm for 20 h under 0.4 MPa argon atmosphere. NaCl to aluminum mole ratio: 0.1-1.5	microparticles, 10 µm – 50 nm; mechanical milling induced defects (dislocations, vacancies, grain boundaries, etc.,)	water	NA	75 mL min^{-1} g^{-1}	[18]
Al and Al alloys	commercial Al powder and Al/Si alloy powder	powder	water, NaOH or KOH	unstable; fast aluminum corrosion	405 289	[19]
Al-Ga-In-Sn-Bi quinary alloy	different ratios of commercial metal powders were prepared and heated at 800 ^oC for 1 h under nitrogen atmosphere	irregular shaped small particles, 20-30 µm; irregular shaped granular particles, 9- 15 µm	water (30 to 60 ^oC)	rapid loss of chemical activity on storage under air is expected.	40 mL min^{-1} g^{-1}	[16]
Al alloys	different ratios of commercial metal powders were prepared and heated at 900 ^oC for 15 min under inert atmosphere	powder, irregular grain sizes	water	rapid loss of activity on storage under air. Storage under liquid N_2 is mandatory to remain the chemical activity.	[d]80 and [e]480 mL g^{-1}	[17]
Porous aluminum electrode	electrochemical (6V, 60 s)	micropores, active zig-zag edges, 3D channels ([b]L = 2.5 cm; [c]D = 1.5 cm)	0.5 and 1.0	stable (900 CV cycles); zig-zag edges are retained; positive potential shifts chronoamperometry : current loss (9% @6.9 mA cm^{-2}; stable for 1 h)	7.5 @ 1.35 V	This work

[a]NA not available; [b] L = length; [c]D = diameter; [d]Al =95%; [e]Al = 90%.

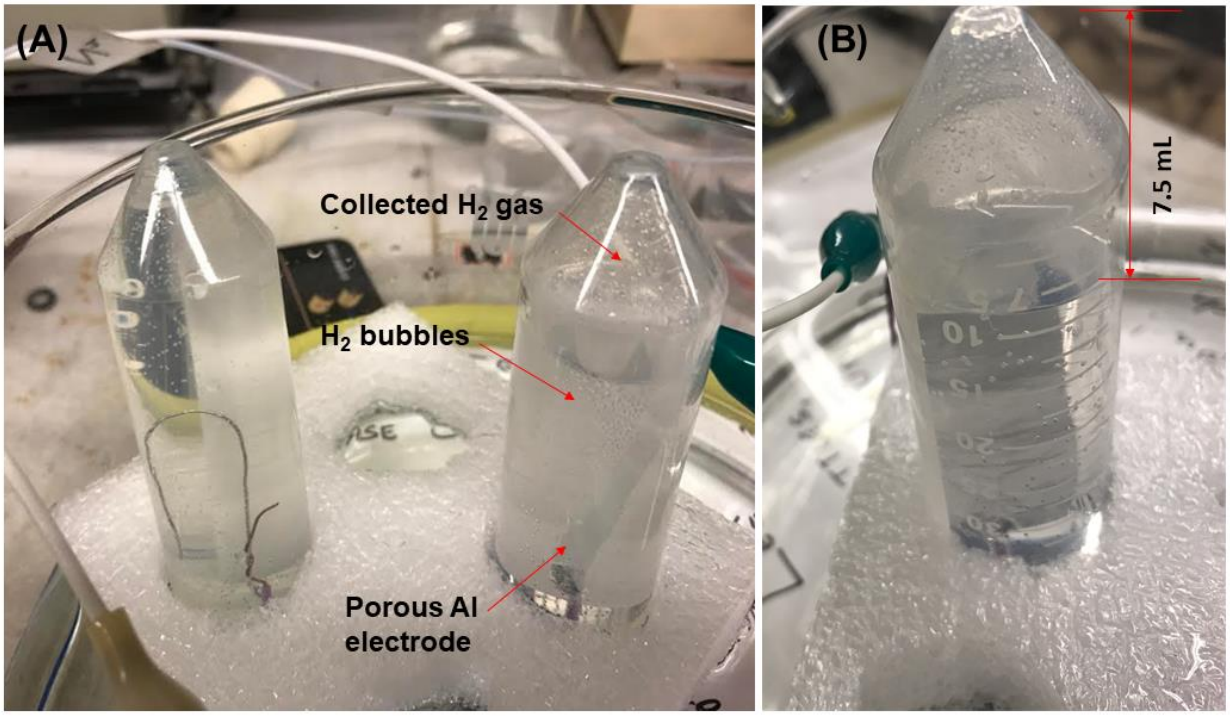

Fig. S9 A custom-built electrochemical cell for hydrogen production using the BAA aluminum electrode. During hydrogen production (A) and after hydrogen production (B) at 1.35 V vs. RHE for 1 h in 1000 mL of 1 M H_2SO_4 (B).

ESI note 5:

Comparison of the porous aluminum electrode with reported ones for HER

The onset overpotential is lower or comparable to other defect-rich catalysts.[24-27] Its overpotential to provide 10 mA cm^{-2} is close to that of defect-rich monolayer MoS_2[26], nitrogen or sulfur doped graphene[28], but it is higher than that of nitrogen and sulfur co-doped graphene[28], defect-rich MoS_2,[29] TM-doped MoS_2[30] and edge oriented MoS_2[25]. Note that the porous aluminum

foil (bulk material) itself was used as a catalyst without any further modification with transition metals (Fe, Co, Mo or Ni), carbon supports (graphene or carbon nanotubes), or dopants. The Tafel slope value of the porous aluminum electrode is smaller than that of many defect-rich transition metal catalysts[24-27, 29-31] and Ni-Al alloy[6], mainly because improved charge transfer and ion/or mass transport through the multiple defects are generated that are responsible for its improved HER performance.[32] Relative to those catalysts, the porous aluminum electrode is cheaper, and it can be prepared with advantages of simplicity, rapidity, green (sustainability), and use of less energy. What we need to prepare porous aluminum electrodes is low-cost aluminum foil, a portable potentiostat, and non-toxic salt (NaCl). It can be prepared within 80 s while applying a voltage at 6 V. If needed, it can be prepared in a shorter time when applying a higher voltage. It is also important to note that the defect structure and electrochemical activity of porous aluminum electrodes can be controlled by varying the anodization potential and time, as well as the species and concentration of salts.

T**able S2.** Comparison of the HER activity of defect-rich non-noble metals in acidic medium.

Electrode	Synthesis (condition)	Defects	H_2SO_4 (M)	Overpotential (η)@10 mA cm^{-2}	E_{onset} of HER (V)	Tafel Slope (mV/ dec)	Ref.
Co-NRCNTs MWCNTs	hydrothermal (700 ° C/2h N_2, post treatment with 0.5 M H_2SO_4, 24h)	N dopant-related structural defects	0.5	0.26	-0.05 -0.44	69 215	[24]
Defect-rich MoS_2	hydrothermal (220 °C/18h)	active edge sites	0.5	0.2	-0.12	50	[29]
[a]TM-doped MoS_2	hydrothermal (600 °C/20 min, Ar, 200 °C, 10 min)	exposed Mo-edges and S-edges	0.5	0.3	-0.2	117	[30]
Edge oriented MoS_2	electrochemical (0.15 M oxalic acid, 25 mA cm^{-2}/20 min), hydrothermal (300 °C, 2 h)	edge oriented defects	0.5	[c]0.3	-0.15 to -0.2	50	[25]
Defect-rich monolayer MoS_2	[b]CVD (750 °C, Ar), oxygen plasma exposure, H_2 post treatment (500 °C/H_2)	cracks and triangular holes	0.5	0.58	-0.3	147	[26]
WS_2(1-0.52) Se_2x nanotubes	hydrothermal (800-1000 °C/60 min, Ar)	layer dislocations and exposed edge sites	1	0.3	-0.28	105	[27]
MoP NPs	hydrothermal (500 °C/10 h, O_2	nanopores	0.5	0.13	-0.04	54	[31]

	and 850 ^{o}C/2h, H_2/Ar)						
N-doped graphene	[c]CVD (800 ^{o}C, 2min), post treatment with 2M HCl, 2h	nanopores, 3D structure	0.5	0.56	-0.4	232	[28]
S-doped graphene				0.48	-0.25	230	
NS co-doped graphene				0.22	-0.39		
NiS_2@Al_2O_3 nanosheets	hydrothermal (180 ^{o}C, 18h), post treatment (750 ^{o}C, 3.2 h) and calcination at 400 ^{o}C, 3.2 h)	porous structure	0.5	0.17	-0.13	42	[21]
Porous aluminum electrode	electrochemical (6V, 60 s)	micropores, active zig-zag edges, 3D channels	1	0.58	-0.46	43	This work

[a]Transition metal doped MoS_2

[b,c] CVD - Chemical vapor deposition

ESI note 6:

Photoelectrochemical hydrogen production of the porous aluminum electrode

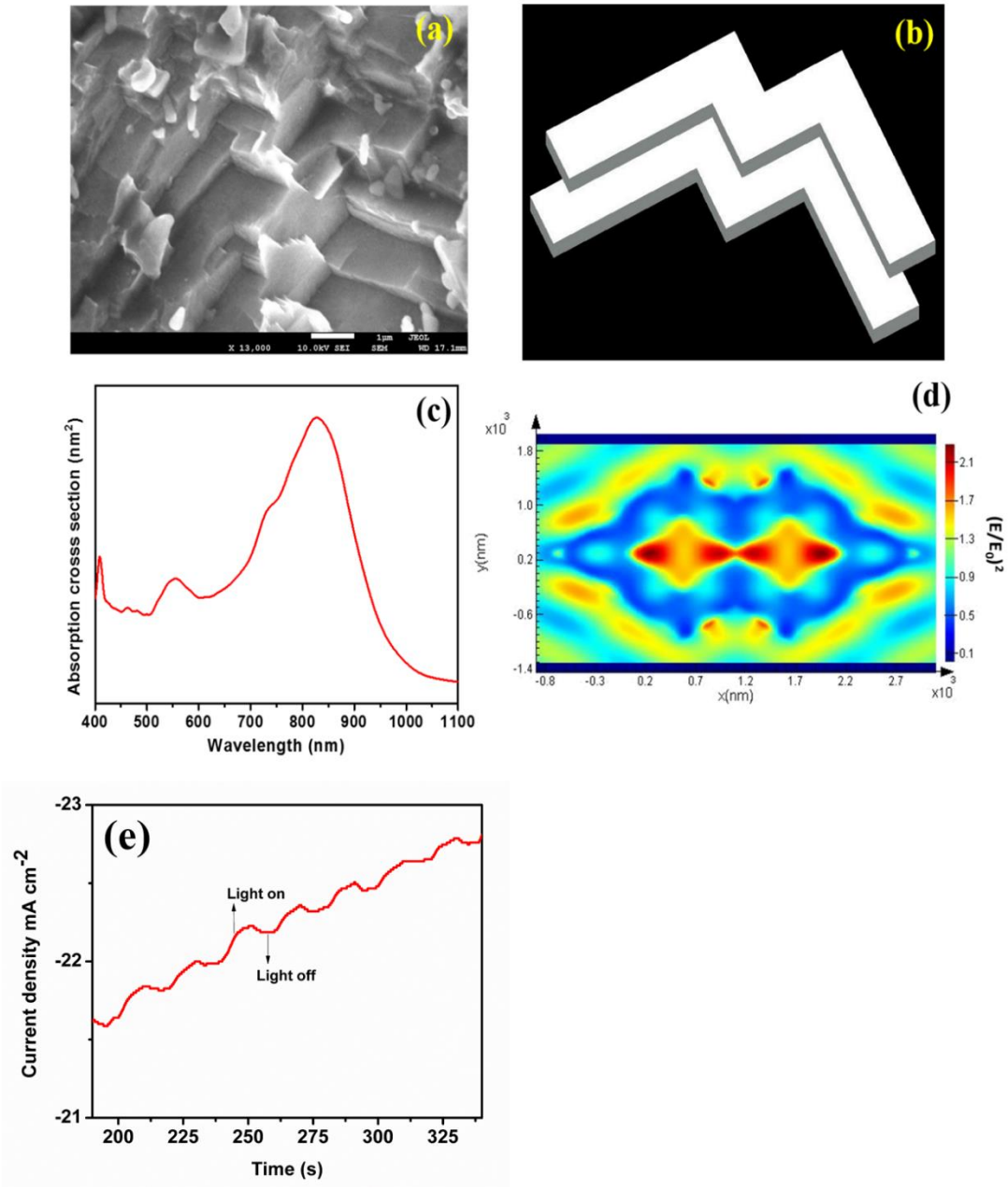

Fig. S10 (a) SEM image showing zig-zag active edges of a BAA aluminum electrode prepared in 60 mM NaCl at 6 V for 80 s; (b) FDTD simulation setup for one unit cell of zig-zag structured defects; (c) Absorption cross section of zig-zag active edges in the electrode; (d) FDTD simulated

XY E-field distribution of zig-zag active edges in the electrode, (e) The photocurrent responses of the electrode measured at an overpotential of 0.82 V vs. RHE under chopped illumination.

Fig. S10a shows the SEM image of zig-zag structured defects in the BAA aluminum electrode. We constructed one unit cell of such zig-zag structures to observe the electric field confinement during light illumination using finite difference time domain (FDTD) simulation (see **Fig. S10b**). The absorption cross section of zig-zag structures displayed in **Fig. S10c** reveals that the zig-zag active edges has resonance around 820 nm. **Fig. S10d** illustrates the e-field distribution of zig-zag defects and the electric field confined around the edges of zig-zag structures that provide electrons for the hydrogen production enhancement. **Fig. S10d** shows the photoresponses of the BAA aluminum electrode measured at an overpotential of 0.82 V under chopped illumination. The sharp spikes in photocurrents during each on/off illumination cycles recorded at a short time interval (10 s) reaveals the fast transport of photogenerated electrons through the active edges, leading to efficient photocatalysis of hydrogen.

References

1. X. Huang, T. Gao, X. Pan, D. Wei, C. Lv, L. Qin and Y. Huang, *J Power Sources,* 2013, **229**, 133-140.
2. P. Natishan and W. O'grady, *J Electrochem. Soc.,* 2014, **161**, C421-C432.
3. L. Liang, Y. He, H. Song, X. Yang, X. Cai, C. Xiong and Y. Li, *Corrosion Science*, 2013, **70**, 180-187.
4. C. M. Brett, I. A. Gomes and J. P. Martins, *Corrosion Science*, 1994, **36**, 915-923.
5. M.-R. Gao, J.-X. Liang, Y.-R. Zheng, Y.-F. Xu, J. Jiang, Q. Gao, J. Li and S.-H. Yu, *Nat. Commun.,* 2015, **6**.
6. A. Rami and A. Lasia, *J Appl. Electrochem.*, 1992, **22**, 376-382.
7. Y. Li, H. Wang, L. Xie, Y. Liang, G. Hong and H. Dai, *J. Am. Chem. Soc,* 2011, **133**, 7296-7299.
8. K. Ogura, *J CO_2 Util.*, 2013, **1**, 43-49.
9. M. R. Singh, Y. Kwon, Y. Lum, J. W. Ager III and A. T. Bell, *J. Am. Chem. Soc.,* 2016, **138**, 13006-13012.
10. D. V. Esposito, S. T. Hunt, A. L. Stottlemyer, K. D. Dobson, B. E. McCandless, R. W. Birkmire and J. G. Chen, *Angew. Chem. Int. Edit.*, 2010, **49**, 9859-9862.
11. T. Yang, M. Du, H. Zhu, M. Zhang and M. Zou, *Electrochim. Acta*, 2015, **167**, 48-54.
12. N. Cheng, S. Stambula, D. Wang, M. N. Banis, J. Liu, A. Riese, B. Xiao, R. Li, T.-K. Sham and L.-M. Liu, *Nat. Commun.*, 2016, **7**, 13638.
13. N. Roy, K. T. Leung and D. Pradhan, *J Phys. Chem. C,* 2015, **119**, 19117-19125.
14. P. Sriram, D. S. Su, A. P. Periasamy, A. Manikandan, S. W. Wang, H. T. Chang, Y. L. Chueh and T. J. Yen, *Adv. Energy Mater.*, 2018, **8**, 1801184.
15. Y. Shen, A. C. Lua, J. Xi and X. Qiu, *ACS Appl. Mater. Interfaces*, 2016, **8**, 3464-3472.
16. T. Huang, Q. Gao, D. Liu, S. Xu, C. Guo, J. Zou and C. Wei, *Int. J. Hydrog. Energy,* 2015, **40**, 2354-2362.
17. O. V. Kravchenko, K. N. Semenenko, B. M. Bulychev and K. B. Kalmykov, *J Alloy and Compd.*, 2005, **397**, 58-62.
18. B. Alinejad and K. Mahmoodi, *Int. J. Hydrog. Energy*, 2009, **34**, 7934-7938.
19. C.-C. Wang, Y.-C. Chou and C.-Y. Yen, *Procedia Eng.*, 2012, **36**, 105-113.
20. S. Razavi-Tousi and J. Szpunar, *Int. J. Hydrog. Energy*, 2013, **38**, 795-806.
21. Y. Feng, H. Zhang, Y. Guan, Y. Mu and Y. Wang, *J Power Sources*, 2017, **348**, 246-254.
22. F. Kargi, *Int. J. Hydrog. Energy*, 2011, **36**, 3450-3456.
23. F. Kargi and E. C. Catalkaya, *Int. J. Hydrog. Energy*, 2011, **36**, 3457-3464.
24. X. Zou, X. Huang, A. Goswami, R. Silva, B. R. Sathe, E. Mikmeková and T. Asefa, *Angew. Chem.*, 2014, **126**, 4461-4465.
25. Y. Yang, H. Fei, G. Ruan, C. Xiang and J. M. Tour, *Adv. Mater.*, 2014, **26**, 8163-8168.
26. G. Ye, Y. Gong, J. Lin, B. Li, Y. He, S. T. Pantelides, W. Zhou, R. Vajtai and P. M. Ajayan, *Nano Lett.*, 2016, **16**, 1097-1103.
27. K. Xu, F. Wang, Z. Wang, X. Zhan, Q. Wang, Z. Cheng, M. Safdar and J. He, *ACS Nano*, 2014, **8**, 8468-8476.
28. Y. Ito, W. Cong, T. Fujita, Z. Tang and M. Chen, *Angew. Chem. Int. Edit.,* 2015, **54**, 2131-2136.
29. J. Xie, H. Zhang, S. Li, R. Wang, X. Sun, M. Zhou, J. Zhou, X. W. D. Lou and Y. Xie, *Adv. Mater.*, 2013, **25**, 5807-5813.
30. H. Wang, C. Tsai, D. Kong, K. Chan, F. Abild-Pedersen, J. K. Nørskov and Y. Cui, *Nano Res.*, 2015, **8**, 566-575.
31. Z. Xing, Q. Liu, A. M. Asiri and X. Sun, *Adv. Mater.*, 2014, **26**, 5702-5707.
32. P. Biesheuvel, Y. Fu and M. Z. Bazant, *Phys. Rev. E*, 2011, **83**, 061507.